Journal of Magnetic Resonance **146,** 188–195 (2000)
doi:10.1006/jmre.2000.2148, available online at http://www.idealibrary.com on IDEAL®

Peptide Internal Motions on Nanosecond Time Scale Derived from Direct Fitting of ^{13}C and ^{15}N NMR Spectral Density Functions

Kevin H. Mayo,[1] Vladimir A. Daragan, Djaudat Idiyatullin, and Irina Nesmelova

Department of Biochemistry, Molecular Biology, and Biophysics, and the Biomedical Engineering Center, 6-155 Jackson Hall, University of Minnesota Health Science Center, 321 Church Street, Minneapolis, Minnesota 55455

E-mail: mayox001@maroon.tc.umn.edu

Received February 15, 2000; revised June 1, 2000

NMR relaxation-derived spectral densities provide information on molecular and internal motions occurring on the picosecond to nanosecond time scales. Using ^{13}C and ^{15}N NMR relaxation parameters [T_1, T_2, and NOE] acquired at four Larmor frequencies (for ^{13}C: 62.5, 125, 150, and 200 MHz), spectral densities $J(0)$, $J(\omega_C)$, $J(\omega_H)$, $J(\omega_H + \omega_C)$, $J(\omega_H - \omega_C)$, $J(\omega_N)$, $J(\omega_H + \omega_N)$, and $J(\omega_H - \omega_N)$ were derived as a function of frequency for ^{15}NH, $^{13}C_\alpha H$, and $^{13}C_\beta H_3$ groups of an alanine residue in an α-helix-forming peptide. This extensive relaxation data set has allowed derivation of highly defined ^{13}C and ^{15}N spectral density maps. Using Monte Carlo minimization, these maps were fit to a spectral density function of three Lorentzian terms having six motional parameters: τ_0, τ_1, τ_2, c_0, c_1, and c_2, where τ_0, τ_1 and τ_2 are correlation times for overall tumbling and for slower and faster internal motions, and c_0, c_1, and c_2 are their weighting coefficients. Analysis of the high-frequency portion of these maps was particularly informative, especially when deriving motional parameters of the side-chain methyl group for which the order parameter is very small and overall tumbling motions do not dominate the spectral density function. Overall correlation times, τ_0, are found to be in nanosecond range, consistent with values determined using the Lipari–Szabo model-free approach. Internal motional correlation times range from picoseconds for methyl group rotation to nanoseconds for backbone N–H, C_α–H, and C_α–C_β bond motions. General application of this approach will allow greater insight into the internal motions in peptides and proteins.

Key Words: **peptide; internal motions; NMR; ^{13}C and ^{15}N relaxation; spectral densities.**

INTRODUCTION

Ever since it was realized that proteins, and biomolecules in general, are not static, but are highly internally flexible systems of atoms or groups of atoms, attempts have been made to develop approaches to derive information on the amplitudes and frequencies of internal motions. NMR relaxation was recognized early on as having the greatest potential to provide the most comprehensive picture of motional amplitudes and frequencies in a protein. An ever increasing number of experimental NMR relaxation parameters, e.g. spin–lattice and spin–spin relaxation rates, nuclear Overhauser effects, ^{13}C multiplet relaxation, dynamics of various spin order, and relaxation experiments in the rotating frame, can be obtained for practically hundreds of ^{13}C and ^{15}N nuclei in a peptide or protein (*1–5*). Most often, such relaxation data are analyzed to derive motional amplitudes of various vectors within a molecule. This is generally accomplished by using some motional model (*5*) or one of the model-free approaches of King and Jardetzky (*6*), Lipari and Szabo (*7*), or Clore *et al.* (*8*), all of which assume overall tumbling of an isotropic molecule.

Model-free approaches are usually parameterized with three or four terms: a correlation time for overall molecular tumbling, τ_0, one or two correlation times for internal motions, τ_i, and an order parameter, S^2. The order parameter provides an index of internal motional restriction and can be expressed in terms of motional amplitude (angular variance), which is more physically meaningful (*5*). Usually such analyses of NMR relaxation data generate accurate, or nearly accurate if anisotropic molecular motions are involved, values only for the overall tumbling correlation time and the order parameter. Internal motional correlation times, however, are normally not accurately determined using these approaches. This is especially true when relaxation data are acquired at only one magnetic field. Most often, internal motional correlation times fall in the range 10 to 100 ps. In reality, internal motions occur on a much broader time scale. Using ^{15}N NMR relaxation data, Clore *et al.* (*9*) found that 32 residues of the protein interleukin-1β display motions on a time scale of 0.5 to 4 ns, slightly less than the overall molecular rotational correlation time of 8.3 ns. Internal motions occurring on the nanosecond time scale have also been observed using other techniques. With the peptide melittin, for example, analysis of fluorescence data revealed anisotropic internal motions of the single tryptophan on a time scale of 0.14 to 0.72 ns (*10*). More recently, Tamura *et al.* (*11*) used solid state deuterium NMR to demonstrate that

[1] To whom correspondence should be addressed. Fax: 612-624-5121.

1090-7807/00 $35.00

the methyl group axes of three methionines in the *Streptomyces* subtilisin inhibitor protein undergo internal motions with correlation times between 0.1 and 10 ns.

By acquiring NMR relaxation data as a function of the Larmor precession frequency, i.e., at multiple magnetic field strengths, numerous spectral density functions like $J(0)$, $J(\omega_{C\text{ or }N})$, $J(\omega_H)$, $J(\omega_H + \omega_{C\text{ or }N})$, and $J(\omega_H - \omega_{C\text{ or }N})$ can be derived, and these are plotted as spectral density maps [$J(\omega)$ vs ω] (*4*, *12*). Spectral density mapping, in particular, has the potential to provide a complete picture of motional frequencies occurring in the picosecond to nanosecond range, for a multitude of bond vectors in a protein or biomolecule in general. While spectral density mapping has been used by some labs, detailed information on internal motional frequencies has not been forthcoming due to the limited number of relaxation terms that had been acquired at one or two magnetic fields.

Here, ^{13}C and ^{15}N NMR relaxation measurements were performed at four magnetic fields and spectral density mapping was done with an 18-residue peptide GFSKAELAKARAAKRGGY, which at low temperature (5°C) forms an α-helical structure stabilized by a hydrophobic staple motif (*13*). To investigate motional frequencies of a residue within the α-helix domain of this peptide, $^{13}C/^{15}N$ isotopically enriched alanine was incorporated synthetically, and $^{13}C/^{15}N$ NMR relaxation experiments (T_1, T_2, and NOE) were performed at four magnetic field strengths (^{13}C frequencies of 62.5, 125, 150, and 200 MHz). This extensive relaxation data set has allowed derivation of the most complete and accurate $^{13}C_\alpha$ and ^{15}NH spectral density maps to date. Spectral density maps were analyzed using a novel approach. Using Monte Carlo minimization, this procedure directly fits the map to a spectral density function expressed in three Lorentzian terms and parameterized with six motional parameters: τ_0, τ_1, τ_2, c_0, c_1, and c_2, where τ_0, τ_1, and τ_2 are correlation times for overall tumbling and for slower and faster internal motions, respectively, and c_0, c_1, c_2 are their weighting coefficients. The time scale of internal motions was found to vary from picoseconds to nanoseconds.

MATERIALS AND METHODS

Using standard Fmoc solid-phase methodology on either a Milligen or Millipore Excell automatic peptide synthesizer (*14*), a peptide having the amino acid sequence GFSKAELAKARAAKRGGY was synthesized with a $^{13}C/^{15}N$-enriched alanine (CIL, Cambridge) at position 10. The peptide was purified by HPLC on a C18 Bondclone (Phenomenex) column using a linear acetonitrile/water gradient. Peptide purity was checked by analytical HPLC and mass spectrometry.

For NMR measurements, the freeze-dried peptide was dissolved in D_2O for ^{13}C relaxation measurements and in a H_2O/D_2O (90/10) mixture for ^{15}N relaxation measurements. The peptide concentration, determined from the dry weight of freeze-dried samples, was 15 mg/ml. The pH was adjusted to pH 6 by adding microliter quantities of NaOD or DCl. NMR relaxation experiments were performed on Varian Inova-500, 600, and 800 NMR spectrometers equipped with triple-resonance probes and on a Bruker AM-250 NMR spectrometer. The temperature was calibrated by using chemical-shift differences of resonances from methanol.

^{13}C spin–lattice relaxation rates were determined by using the direct homonuclear inversion-recovery method using a composite 180° pulse (90°_x–180°_y–90°_x). In all experiments, broadband ^1H-decoupling GARP (*15*) was used. The number of acquisitions was chosen to give a signal-to-noise ratio greater than 10. Therefore, the number of transients varied from 200 to 1000. Ten to fifteen time-incremented (partially relaxed) spectra were routinely acquired for each relaxation measurement. Relaxation rates were determined by the method described in (*16*). ^{13}C–{^1H} NOE coefficients were measured by using the standard gated decoupling technique.

^{15}N spin–lattice and spin–spin relaxation rates were measured using versions of the HSQC pulse sequence as described by Farrow *et al.* (*17*). The HSQC sequence employs pulsed field gradients for the coherence transfer pathway whereby magnetization passes from ^1H to ^{15}N and back again to ^1H for observation and uses the water flip-back technique to minimize water saturation during the experiment. Following magnetization transfer from ^1H to ^{15}N (INEPT), the ^{15}N spin state population difference is increased, and spin–lattice relaxation occurs during the subsequent time delay prior to magnetization transfer from ^{15}N back to ^1H for detection. For spin–spin relaxation, the CPMG pulse sequence (τ_{CPMG} = 0.45 ms) was employed between INEPT transfer steps. To suppress cross-correlation effects between ^1H–^{15}N dipoles and ^{15}N chemical-shift anisotropy relaxation mechanisms (*17–19*), ^1H 180° shaped pulses (cosine-modulated rectangular) (*20*) and alternating phase 180° ^1H pulses synchronized with the CPMG pulse sequence were applied during spin–lattice and spin–spin relaxation delays, respectively, as described by Farrow *et al.* (*17*).

^{13}C spin–spin (transverse) relaxation rates were also measured by using the CPMG-HSQC method (*17*) described above, with some modifications. Since each ^{13}C nucleus in a given residue has at least one ^{13}C neighbor, homonuclear J coupling causes modulation of the spin-echo decay (*21–23*), thus preventing an accurate measurement of the T_2 relaxation time by using the CPMG pulse sequence. Using soft rectangular pulses (714 to 1250 Hz) applied at the resonance frequency of a given ^{13}C nucleus and a short pulse delay (τ_{CPMG} = 0.45 ms) in the CPMG pulse train eliminated effects from J coupling and permitted the measurement of smooth transverse magnetization decay curves. During the relaxation period, the broadband decoupling WALTZ scheme (*24*) was used. Even though these modifications require performing separate experiments for each nucleus in the sample and increases the measurement time, more reliable and accurate transverse relaxation data were achieved.

Steady-state {^{1}H–^{15}N} and {^{1}H–^{13}C} NOEs were determined from spectra recorded in the presence and absence of proton saturation (*17*). Saturation was achieved by applying 120° ^{1}H pulses every 5 ms during the 5-s preparation period (*25*). In the absence of proton saturation, the relaxation delay (preparation period) was 10 s. This relatively long relaxation delay was sufficient to avoid saturation transfer from water to amide protons (*26*). Five sets of spectra were recorded in this way, and NOE data were averaged.

Spectral densities at different frequencies were determined using a Monte Carlo minimization protocol which minimized the function (*16*)

$$\chi^2 = \sum_i [(W^i_{1\text{exp}} - W^i_{1\text{theor}})/W^i_{1\text{exp}}]^2 + [(W^i_{2\text{exp}} - W^i_{2\text{theor}})/W^i_{2\text{exp}}]^2 + [(NOE^i_{\text{exp}} - NOE^i_{\text{theor}})/NOE^i_{\text{exp}}]^2, \quad [1]$$

where $W^i_{1\text{exp}}$, $W^i_{2\text{exp}}$, and NOE^i_{exp} are the experimental values and $W^i_{1\text{theor}}$, $W^i_{2\text{theor}}$, and NOE^i_{theor} are the calculated values of the NMR relaxation parameters which can be expressed in terms of spectral densities,

$$W_1 = \frac{1}{10} k_{dd}[J(\omega_C - \omega_H) + 3J(\omega_C) + 6J(\omega_C + \omega_H)] + \frac{2}{15}\Delta\sigma^2\omega_C^2 J(\omega_C) \quad [2a]$$

$$W_2 = \frac{1}{20} k_{dd}[J(\omega_C - \omega_H) + 3J(\omega_C) + 6J(\omega_C + \omega_H) + 4J(0) + 6J(\omega_H)] + \frac{1}{45}\Delta\sigma^2\omega_C^2[4J(0) + 3J(\omega_C)] + W_{ex} \quad [2b]$$

$$NOE = \frac{1}{10}\frac{\gamma_H}{\gamma_C}\frac{k_{dd}[6J(\omega_C + \omega_H) - J(\omega_C - \omega_H)]}{W_1}, \quad [2c]$$

where $k_{dd} = n\gamma_C^2\gamma_H^2\hbar^2/r_{CH}^6$; γ_C, γ_H are the magnetogyric ratios for ^{13}C and ^{1}H nuclei; $\hbar$ is the Plank's constant, r_{CH} is the length of the CH bond; and n is the number of attached protons. These equations have been expressed for ^{13}C nuclei; similar equations can be written for ^{15}N. Chemical-shift anisotropy, $\Delta\sigma$, was estimated to be -160 ppm for ^{15}N and -25 ppm for ^{13}C (*2*). In any event, contributions from ^{13}C CSA are much smaller than contributions from ^{13}C–^{1}H dipole–dipole interactions even at the high field (~5%) (*2*). Therefore, this contribution was neglected during data analysis. For CH_2 and CH_3 groups, equations for the NOE are more complicated (*5*). During minimization, it was taken into account that the chemical exchange term, W_{ex}, is proportional to the Larmor frequency squared. The summation in Eq. [1] was performed over all the NMR frequencies for which data were available. By using the following properties of spectral densities, errors in the Monte Carlo minimization procedure were substantially reduced:

$$J(\omega) < J(0) \quad [3a]$$

$$J(\omega_i) < J(\omega_j) \text{ if } \omega_i > \omega_j \quad [3b]$$

$$J(\omega_i)/J(\omega_j) < (\omega_j/\omega_i)^2 \quad [3c]$$

$$\int_0^\infty J(\omega)d\omega = \frac{\pi}{2}. \quad [3d]$$

This last condition establishes the criterion, $\Sigma J(\omega_{i+1})\Delta\omega_i > \pi/2$, for dismissing poor minimization runs.

THEORETICAL CONSIDERATIONS

Spectral densities, $J(\omega)$, can be written in general as the sum of Lorentzian terms

$$J(\omega) = \sum_{i=0}^{N} \frac{c_i\tau_i}{1 + (\omega\tau_i)^2}, \quad [4]$$

where c_i are weighting coefficients with

$$\sum_{i=0}^{N} c_i = 1. \quad [5]$$

For complicated motions, the number of terms N can be very large. The corresponding correlation function is expressed as

$$C(t) = \sum_{i=0}^{N} c_i e^{-t/\tau_i}. \quad [6]$$

For isotropic molecular tumbling and a single term to describe all internal motions, $C(t)$ can be approximated by the Lipari–Szabo equation (*7*)

$$C(t) = S^2 e^{-t/\tau_0} + (1 - S^2)e^{t/\tau}, \quad [7]$$

where S^2 is the well-known order parameter, τ_0 is the correlation time for overall tumbling, and $\tau = \tau_0\tau_i/(\tau_0 + \tau_i)$ with τ_i being the correlation time for internal bond rotations.

With the addition of a second term to describe internal motions, $C(t)$ can be approximated by (*8*)

$$C(t) = e^{-t/\tau_0}S^2 + (1 - S_f^2)e^{t/\tau_{0f}} + (S_f^2 - S^2)e^{t/\tau_{0s}} \quad [8]$$

with $\tau_{0f} = \tau_0\tau_f/(\tau_0 + \tau_f)$ and $\tau_{0s} = \tau_0\tau_s/(\tau_0 + \tau_s)$. τ_s and τ_f are correlation times for relatively fast and slow internal motions. S_f^2 is the order parameter for fast internal motions.

For anisotropic molecular tumbling, $C(t)$ becomes very complicated even when considering only one term to describe all internal motions. A single-order parameter cannot completely characterize internal motional restrictions (*27*). For overall tumbling of a symmetric top, $C(t)$ can be written for a given motional vector **a** as

$$C_{\mathbf{a}}(t) = \sum_{m=0}^{2} [S^2\xi_{m1} + \langle x^2 - y^2\rangle\xi_{m2} + ((1 - S^2)\xi_{m3} + \langle x^2 - y^2\rangle\xi_{m4})e^{-t/\tau}]e^{-D_m t} \quad [9]$$

with the diffusion coefficients D_m being

$$D_m = 6D_\perp + (D_\parallel - D_\perp)m^2. \quad [10]$$

Here, $D_\parallel$ and $D_\perp$ are rotational diffusion coefficients for rotations about the molecular symmetry axis and about an axis that is perpendicular to that symmetry axis, respectively. Coefficients ξ_{mk} depend upon the orientation of vector **a** within the molecular frame (*5*), S^2 is identical to the order parameter for isotropic overall tumbling, and τ is the correlation time for internal motions. The parameter $\langle x^2 - y^2\rangle$ is the second restriction parameter used to describe the anisotropy of internal bond rotations. x and y are projections of the unit motional vector **a** onto the plane that is perpendicular to the average position of vector **a** in the molecular frame. In this plane, the y axis runs perpendicular to the plane (Z_D, $\langle\mathbf{a}(t)\rangle$) where Z_D is the symmetry axis of the molecular (diffusion) frame and $\langle\mathbf{a}(t)\rangle$ is the average position of motional vector **a**. S^2 is related to $\langle x^2 + y^2\rangle$ as $S^2 = 1 - 3\langle x^2 + y^2\rangle$ (*27*). Therefore, for overall tumbling of a symmetric top, only two restriction parameters, $\langle x^2\rangle$ and $\langle y^2\rangle$, are required to describe internal motions.

These examples demonstrate the complexity of interpreting NMR relaxation data. Using the Lipari–Szabo model-free approach can lead to significant inaccuracies in deriving internal motional parameters. There are two ways to minimize such errors. One is to use a more complex motional model that contains as few motional parameters as possible. For anisotropic overall tumbling, the normally required 23 parameters required to describe the 12 Lorentzian terms in Eq. [9] can be reduced to 5 parameters: $D_\parallel$, $D_\perp$, $\langle x^2\rangle$, $\langle y^2\rangle$, and τ. The second way is to directly analyze the complete spectral density map (*4, 12*) that has been derived from NMR relaxation parameters acquired at different magnetic fields. Only considering ^{13}C–H dipole–dipole interactions, relaxation rates and NOEs determined at each magnetic field can be described in terms of spectral densities at five frequencies: $J(0)$, $J(\omega_C)$, $J(\omega_C - \omega_H)$, $J(\omega_C + \omega_H)$, and $J(\omega_H)$. Even though the number of spectral densities is larger than the number of experimental parameters, acquiring relaxation data at four magnetic fields allows highly accurate spectral density maps to be determined. This later approach is used here.

ANALYSIS OF SPECTRAL DENSITY FUNCTIONS

Initially, analysis of the high-frequency region of spectral densities was performed. At high frequencies where τ is large, spectral density terms $\tau/(1 + \omega^2\tau^2)$ are reduced to $1/(\omega^2\tau)$ and the spectral density function (Eq. [3] in three terms) can be expressed as

$$J(\omega) \approx \left(\frac{c_0}{\tau_0} + \frac{c_1}{\tau_1}\right)\frac{1}{\omega^2} + \frac{c_2\tau_2}{1 + (\tau_2\omega)^2}. \quad [11]$$

When the curve of $J(\omega)$ vs $1/\omega^2$ is linear, $(\omega\tau_2)^2 \ll 1$ and the third term in Eq. [11] can be approximated as $c_2\tau_2$, yielding

$$J(\omega) \approx \left(\frac{c_0}{\tau_0} + \frac{c_1}{\tau_1}\right)\frac{1}{\omega^2} + c_2\tau_2. \quad [12]$$

The slope of this linear line is equal to $(c_0/\tau_0 + c_1/\tau_1)$, and the Y-axis intercept is equal to $c_2\tau_2$.

At the highest field used in these relaxation experiments, the upper frequency limit for $J(\omega)$, i.e., $(\omega_H + \omega_C)$, is about 1000 MHz. Since this is the nanosecond time scale, deviation from linearity in curves of $J(\omega)$ vs $1/\omega^2$ is expected when τ_1 falls in the range 100 to 300 ps. In this case, the curve may be approximated using a parabolic curve such that

$$J(x) \approx c_2\tau_2 + \left(\frac{c_0}{\tau_0} + \frac{c_1}{\tau_1}\right)x - \left(\frac{c_0}{\tau_0^3} + \frac{c_1}{\tau_1^3}\right)x^2, \quad [13]$$

where $x = 1/\omega^2$. To exemplify this, consider the case where $\tau_0 = 2$ ns, $c_0 = 0.7$, $\tau_1 = 0.3$ ns, $c_1 = 0.15$, $\tau_2 = 20$ ps, and $c_2 = 0.15$. Figure 1 plots calculated values for $J(\omega)$ using Eq. [4] with three Lorentzians and no approximations (filled-in circles) and Eq. [13] (open circles). For frequencies greater than 800 MHz, the difference between these curves is minimal and the parabolic approximation yields $c_2\tau_2$ (Y-axis intercept) with excellent accuracy. Therefore, use of Eq. [13] provides an opportunity to estimate internal correlation times for motions occurring on a relatively fast time scale. This approach is of particular advantage in analyzing internal motions of methyl groups for which the coefficients c_0 and c_1 are small and c_2 is close to 1.

The full spectral density maps were then fitted to Eq. [3] with three Lorentzian terms using Monte Carlo minimization to determine the six motional parameters: τ_0, τ_1, τ_2, c_0, c_1, and c_2. τ_0, τ_1, and τ_2 are correlation times for overall tumbling and for slower and faster internal motions, respectively, and the sum of weighting coefficients $c_0 + c_1 + c_2 = 1$. For isotropic molecular motion, c_0 is the Lipari–Szabo order parameter S^2.

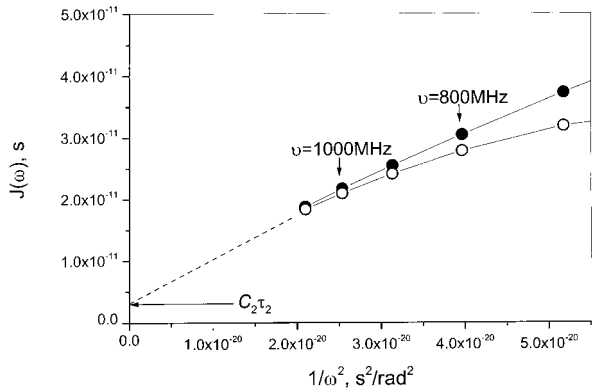

FIG. 1. The high-frequency region of the spectral density map has been calculated using a spectral density function expressed in three Lorentzian terms. Filled-in circles are the results of calculations using Eq. [4], and open circles are the result of calculations using Eq. [13]. In either case, calculations were made with $\tau_0 = 2000$ ps, $\tau_1 = 300$ ps, $\tau_2 = 20$ ps, $c_0 = 0.7$, and $c_1 = c_2 = 0.15$. Solid lines result from fitting with a parabolic curve.

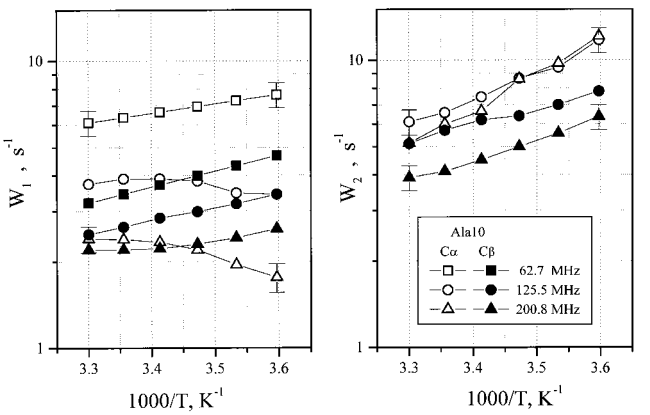

FIG. 2. The temperature and frequency dependence of spin–lattice and spin–spin relaxation rates, W_1 and W_2, respectively, are shown for $^{13}C_\alpha$, $^{13}C_\beta$, and ^{15}N nuclei of alanine A10 in the α-helical region of the peptide. Experimental errors determined from linear regression fits to the relaxation curves are less than 5 to 10% as exemplified by error bars shown for a few data points in the figure.

In the fitting procedure, c_2 was calculated from $c_2 = 1 - c_0 - c_1$; therefore only five parameters had to be determined. Prior to minimization, initial values for τ_0 and c_0 were derived using the Lipari–Szabo approach with $c_0 = S^2$, and for the alanine $C_\beta H_3$ group, an initial value for τ_2 was estimated by analyzing the spectral density map at high frequencies to derive the first term in Eq. [13], which is the Y-axis intercept of $J(\omega)$ vs $1/\omega^2$. Since for methyl groups, c_2 is close to 1, τ_2 can be determined fairly accurately using this approach. During minimization, it was assumed that $0 < \tau_2 < \tau_1 < \tau_0$, and for the methyl group, it was known that c_0 had to be in the range $0 < c_0 < 0.11$. The number of steps in the Monte Carlo calculation was more than 5×10^6. Errors were estimated by determining values for $J(\omega)$ based on spin–lattice and spin–spin relaxation rates and NOEs acquired at four magnetic fields (^{13}C frequencies of 62.5, 125, 150, and 200 MHz). These relaxation rates were calculated by approximating the spectral density function in Eq. [3] with three Lorentzian terms as described above. Using this procedure, $J(0)$ was determined with an accuracy of 0.3%, and $J(\omega)$ at high frequency had an accuracy of 3 to 5%. In this regard, the main source of error in $J(\omega)$ arose from errors in experimental parameters and not from the minimization procedure.

RESULTS AND DISCUSSION

For $^{13}C/^{15}N$-enriched A10 in the α-helix-forming peptide GFSKAELAKARAAKRGGY (*13*), spin–lattice (T_1) and spin–spin (T_2) relaxation times and heteronuclear NOEs were measured at four Larmor precession frequencies (^{13}C frequencies of 62.5, 125, 150, and 200 MHz) and at temperatures of 5, 15, and 30°C. Some of these relaxation data are plotted in Fig. 2 to show the quality of the data. With these relaxation rates, spectral densities $J(0)$, $J(\omega_C)$, $J(\omega_H)$, $J(\omega_H + \omega_C)$, $J(\omega_H - \omega_C)$, $J(\omega_N)$, $J(\omega_H + \omega_N)$, and $J(\omega_H - \omega_N)$ were determined using Monte Carlo minimization as described in the previous section. Spectral density maps are shown in Fig. 3 for $^{13}C_\alpha H$, $^{13}C_\beta H$, and ^{15}NH of A10. At low and high frequencies, errors are estimated to be 0.5 and 3%, respectively. The accuracy of these spectral density functions is well within the size of the symbols shown, with the main source of error in $J(\omega_i)$ arising from experimental errors in the relaxation parameters.

At zero frequency, the spectral density $J(0)$ for the NH bond is slightly larger than that for the $C_\alpha H$ bond. This most likely results from anisotropic molecular motion. At 5°C, this peptide is about 50% helical with the helix (determined by analysis of

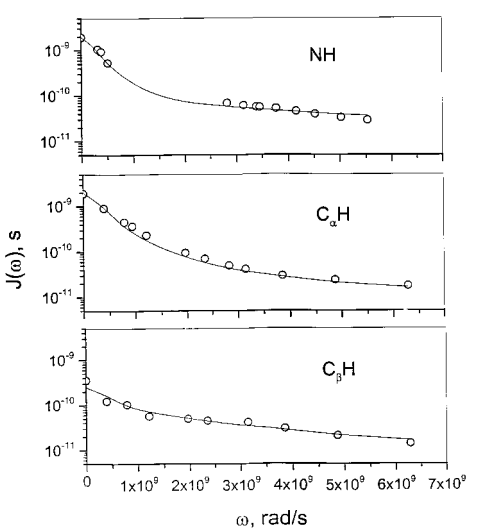

FIG. 3. Spectral densities for ^{15}NH, $^{13}C_\alpha H$, and $^{13}C_\beta H$ bonds of alanine A10 in the α-helical peptide at 5°C are plotted versus frequency. Solid lines are the result of directly fitting the spectral density maps with a spectral density function having three Lorentzian terms parameterized with six motional parameters as discussed in the text.

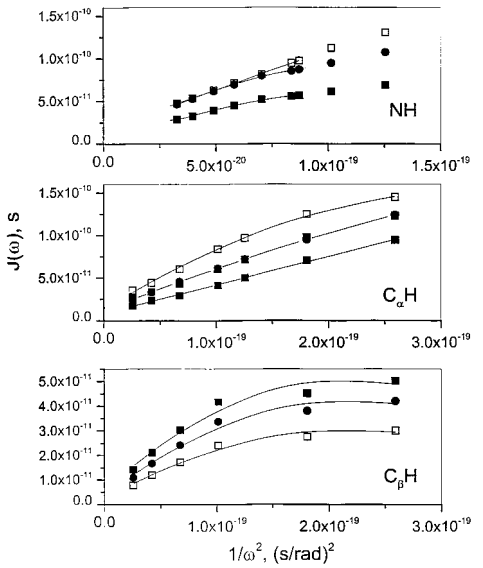

FIG. 4. The high-frequency region of spectral density maps for ^{15}NH, $^{13}C_\alpha H$, and $^{13}C_\beta H$ have been plotted as $J(\omega)$ vs $1/\omega^2$. Data for three temperatures are shown: 5°C (filled-in squares), 15°C (filled-in circles), and 30°C (open squares). Solid lines are the result of directly fitting the spectral density maps with a spectral density function having three Lorentzian terms parameterized with six motional parameters as discussed in the text.

^{1}H NOEs and computational modeling) running from A5 to A13 (*13*). The shape of the peptide in this folded state is better approximated as a cylinder rather than a sphere. In the helix conformation, the angle that the A10 NH bond makes with respect to the main axis of the helix is, on average, 11°, whereas the angle that the $C_\alpha H$ bond makes with respect to the main axis of the helix is 58°. In this regard, the NH bond is nearly parallel to the helix dipole axis making its correlation time somewhat longer than that of the $C_\alpha H$ bond. The ratio of $J(0)$ for ^{15}NH to $J(0)$ for $^{13}C_\alpha H$ is 1.1 to 1.2 and is fairly stable showing little temperature dependence from 5 to 30°C.

The high-frequency regions of these spectral density functions are plotted in Fig. 4 as $J(\omega)$ vs $1/\omega^2$ at three temperatures. The solid line fits are the result of parabolic approximation as described in the previous section. Differences between $C_\alpha H$ and NH spectral densities are apparent. At lower temperature (5°C), the curve $J(\omega)$ vs $1/\omega^2$ for the NH bond is less linear than that for the $C_\alpha H$ bond. This indicates that NH bond motional correlation times τ_1 and τ_2 are larger than those for the $C_\alpha H$ bond. At 30°C, the effect is reversed and nonlinearity is greater for $C_\alpha H$. Over this same high-frequency range, spectral densities for $C_\beta H$ are even more nonlinear and decrease, not increase, with increasing temperature. For $C_\beta H$, linearity in $J(\omega)$ vs $1/\omega^2$ is observed only at the highest frequencies. These differences are related to the fact that for methyl group $C_\beta H$ bonds, contributions from slower motions are relatively minimal because the order parameter for the methyl CH bonds can be expressed as $S^2 = 1/9 S^2_{CC}$, where S^2_{CC} is the order parameter for fluctuations of the methyl group symmetry axis, i.e., the C_α–C_β bond. The coefficient 1/9 substantially reduces the contribution from overall molecular tumbling and the terms with τ_1 and τ_2 dominate the spectral density function. Qualitatively, this explains the differences in the behavior of $C_\alpha H$, NH, and $C_\beta H$ spectral densities shown in Fig. 4. For the methyl group, therefore, analysis of this high-frequency region using Eqs. [12] or [13] allows initial estimates of τ_2 for use in fitting the complete spectral density map.

Using initial estimates for τ_0 and c_0 [for C_α, C_β, and NH] derived using the Lipari–Szabo approach (*7*) as well as estimates for τ_1, τ_2, c_1, and c_2 derived for the methyl group as described above, coefficients c_0, c_1, c_2 and correlation times τ_0, τ_1, τ_2 were determined by fitting the complete spectral density maps in Fig. 3 with the three Lorentzian approximation of Eq. [3] using Monte Carlo minimization. These fits are shown as solid lines in Fig. 3, and derived motional parameters at 5 and 30°C are presented in Table 1. As expected, the correlation time for overall tumbling, τ_0, fell in the 2.5 ns range at 5°C and decreased to 1 to 1.8 ns at 30°C. Moreover, c_0 for NH and $C_\alpha H$ is between 0.55 and 0.8 at either temperature. Remember that in the Lipari–Szabo (*7*) and Clore *et al.* (*8*) isotropic motional models, c_0 is the order parameter S^2. These values for τ_0 and c_0 provide increased confidence that this analytical approach can yield reasonable and meaningful correlation times and weighting coefficients. This conclusion is further supported by values derived for τ_2 and c_2 for the alanine $C_\beta H_3$ group. These faster motion terms should be associated with methyl group rotations about the C_α–C_β bond and would be expected to dominate the spectral density function for the methyl carbon. As shown in Table 1, c_2 for $C_\beta H_3$ is the largest of the three weighting coefficients, and τ_2 falls in the very fast motion range of 10 ps.

Of greater note, however, are values derived for motional correlation times τ_1 (Table 1). Analyses using standard motional models, like those of Lipari–Szabo (*7*) and Clore *et al.* (*8*), and NMR relaxation data acquired at a single magnetic field usually yield inaccurate, internal motional correlation times under 100 ps. For this helical peptide at 5°C, τ_1 values given in Table 1 are near-nanosecond. However, since the structured peptide is not spherical, molecular anisotropy may contribute to these τ_1 values. To assess the contribution from molecular anisotropy to τ_1, an anisotropic motional model initially formulated by Favro (*28*) and expressed for NMR relaxation data by Woessner (*29*) and later modified by Huntress (*30*) was employed. Using the ratio of components of the rotational diffusion tensor, which for this helical peptide was estimated by the Kirkwood–Steel–Huntress theory (*5*) to be 2.7 (the value for a symmetric top), the Woessner symmetric top model for anisotropic tumbling (*30*) yielded $\tau_1 \approx 0.75\ \tau_0$. The value of τ_1/τ_0 ($\approx$0.75) is much larger than that determined experimentally. For NH, $\tau_1/\tau_0 = 0.3$ at 5°C and 0.55 at 30°C. For $C_\alpha H$, $\tau_1/\tau_0 = 0.13$ at 5°C and 0.55 at 30°C. Since τ_1/τ_0 is smaller at lower temperature where the peptide is more structured, molecular anisotropy, if anything, should contribute

TABLE 1
Overall and Internal Motional Correlation Times and Weighting Parameters: τ_0, τ_1, τ_2, c_0, c_1, and c_2

Bond	τ_0	c_0	τ_1	c_1	τ_2	c_2
			Temperature, 5°C			
$C_\alpha H$	2300 ± 200	0.8 ± 0.1	300 ± 200	0.1 ± 0.05	50 ± 30	0.1 ± 0.05
$C_\beta H$	2000 ± 300	0.06 ± 0.02	300 ± 200	0.09 ± 0.06	8 ± 2	0.8 ± 0.1
NH	2600 ± 300	0.55 ± 0.1	800 ± 300	0.15 ± 0.1	300 ± 150	0.3 ± 0.15
			Temperature, 30°C			
$C_\alpha H$	1100 ± 100	0.55 ± 0.07	600 ± 200	0.1 ± 0.05	30 ± 20	0.35 ± 0.1
$C_\beta H$	1800 ± 400	0.04 ± 0.01	500 ± 200	0.09 ± 0.06	4 ± 1	0.85 ± 0.05
NH	1100 ± 300	0.6 ± 0.1	600 ± 200	0.1 ± 0.05	200 ± 100	0.3 ± 0.15

Note. τ_0, τ_1, and τ_2 are correlation times for overall tumbling and for slower and faster internal motions, and c_0, c_1, and c_2 are their weighting coefficients. These terms result from the use of Monte Carlo minimization to directly fit spectral density maps with a spectral density function expressed in three Lorentzian terms parameterized with these six motional parameters. Data are given for ^{15}NH, $^{13}C_\alpha H$, and $^{13}C_\beta H$ of alanine A10 in an α-helix-forming peptide at 5 and at 30°C.

more to the ratio τ_1/τ_0, and it does not. This indicates that τ_1 arises primarily from internal motions. In addition, coefficients from the Woessner model contain $\sin^2(\theta)$ and $\sin^4(\theta)$ terms. θ is the angle between a given bond vector and the symmetry axis of the helix. Particularly for an NH bond in an α-helix, this angle is small, making these sine terms and coefficients extremely small such that contributions from molecular anisotropy become negligible. Together, these arguments indicate that correlation times τ_1 and τ_2 are mostly attributable to internal motions and not to anisotropic overall tumbling.

For this helical peptide, τ_1 values for both backbone C_α–H and N–H bond vectors are in the range 0.4 to 0.8 ns (Table 1). Moreover, since τ_1 for $C_\beta H$ is essentially the same as that for $C_\alpha H$, it can be interpreted as the correlation time for C_α–C_β bond fluctuations. This means that all three motional vectors [N–H, C_α–H, and C_α–C_β], originating from backbone positions, display essentially the same τ_1 values within error. Although the physical nature of these slow fluctuations of backbone groups is unknown, the nanosecond time scale is consistent with the occurrence of larger amplitude and/or more complicated, concerted motions. An upper limit to the time scale for such motions may be taken as the peptide folding–unfolding event, which ranges from tenths of microseconds for a helical peptide to microseconds for a β-hairpin peptide (*31*, *32*). Being two to three orders in magnitude smaller than this, these τ_1 values are probably the result of local, concerted motions involving multiple bond rotations, like correlated ϕ, ψ bond rotations (*33*). Note also that τ_2 for the NH group is also large, suggesting that internal motions of the backbone NH are more complicated than those of C_α–H and C_α–C_β. Hydrogen bond formation between backbone N–H and C═O groups within the helix may be partly responsible for this. It is also interesting to note that unlike τ_2 values which decrease with increasing temperature, τ_1 values at 5°C are on the same order as those at 30°C, even though the structured population is highly reduced at the higher temperature. This observation that internal motions in this less folded state still occur on the same nanosecond time scale as in the more folded state supports the idea that at 30°C, the peptide exists in a collapsed, yet highly transient, state (*34*, *35*).

CONCLUSIONS

NMR relaxation data (^{13}CH and ^{15}NH T_1, T_2, and NOE) acquired at four magnetic field strengths have allowed derivation of the most complete and accurate $^{13}C_\alpha H$ and ^{15}NH spectral density maps reported to date on any biomolecule. Direct fits to these spectral density maps, moreover, have provided unique information on near-nanosecond internal motions of backbone bonds in an α-helix-forming peptide. In general, spectral density mapping should be more informative for larger peptides where the decay due to overall tumbling will be less effective at higher frequencies and internal motions can be studied in greater detail.

ACKNOWLEDGMENTS

This work was supported by research grants from the National Science Foundation (MCB-9729539) and the National Institutes of Health (GM-58005). NMR instrumentation was made possible with funds from the NSF (BIR-961477) and the University of Minnesota Medical School.

REFERENCES

1. G. M. Clore and A. M. Gronenborn (Eds.), "NMR of Proteins," CRC Press, Boca Raton (1993).
2. J. W. Peng and G. Wagner, Investigation of protein motions via relaxation measurements, *Methods Enzymol.* **239,** 563–596 (1994).
3. R. Brueschweiler and D. A. Case, Characterization of biomolecular structure and dynamics by NMR cross relaxation, *Prog. NMR Spectrosc.* **26,** 27–58 (1994).

4. K. T. Dayie and G. Wagner, Theory and practice of nuclear spin relaxation in proteins, *Ann. Rev. Phys. Chem.* **47,** 243–282 (1996).
5. V. A. Daragan and K. H. Mayo, Motional model analyses of protein and peptide dynamics using ^{13}C and ^{15}N NMR relaxation, *Prog. NMR Spectrosc.* **32,** 63–105 (1997).
6. R. King and O. Jardetzky, A general formalism for the analysis of NMR relaxation measurements on systems with multiple degrees of freedom, *Chem. Phys. Lett.* **55,** 15–18 (1978).
7. G. Lipari and A. Szabo, Model-free approach to the interpretation of nuclear magnetic resonance relaxation in macromolecules. II. Analysis of experimental results, *J. Am. Chem. Soc.* **104,** 4559–4570 (1982).
8. G. M. Clore, A. Szabo, A. Bax, L. E. Kay, P. C. Driscoll, and A. M. Gronenborn, Deviations from the simple two-parameter model free approach to the interpretation of ^{15}N nuclear magnetic relaxation of proteins, *J. Am. Chem. Soc.* **112,** 4989–4991.
9. G. M. Clore, P. C. Driscoll, P. T. Wingfield, and A. M. Gronenborn, Analysis of the backbone dynamics of interleukin-1β using two-dimensional inverse heteronuclear ^{15}N-^{1}H NMR spectroscopy, *Biochemistry* **29,** 7387–7401 (1990).
10. J. R. Lakowicz, H. Cherek, I. Gryczynski, N. Joshi, and M. L. Johnson, Enhanced resolution of fluorescence anisotropy decays by simultaneous analysis of progressively quenched samples. Applications to anisotropic rotations and to protein dynamics, *Biophys. J.* **51,** 755–768 (1987).
11. A. Tamura, M. Matsushita, A. Naito, S. Kojima, K. I. Miura, and K. Akasaka, Dynamics of the three methionyl side-chains of *Streptomyces* subtilisin inhibitor. Deuterium NMR studies in solution and in the solid state, *Protein Sci.* **5,** 127–139 (1996).
12. J. W. Peng and G. Wagner, Mapping of the spectral densities of N-H bond motions in eglin c using heteronuclear relaxation experiments, *Biochemistry* **31,** 8571–8586 (1992).
13. V. Munoz, F. J. Blanco, and L. Serrano, The hydrophobic-staple motif and a role for loop-residues in α-helix stability and protein folding, *Struct. Biol.* **2,** 380–385 (1995).
14. E. Atherton and R. C. Sheppard, "Solid Phase Peptide Synthesis: A Practical Approach," IRL Press, Oxford, UK (1989).
15. A. J. Shaka, P. B. Barker, and R. Freeman, Computer-optimized decoupling scheme for wideband applications and low-level operation, *J. Magn. Reson.* **64,** 547–552 (1985).
16. V. A. Daragan, M. A. Kloczewiak, and K. M. Mayo, ^{13}C nuclear magnetic resonance relaxation-derived psi, phi bond rotational energy barriers and rotational restrictions for glycine ^{13}C alpha-methylenes in a GXX-repeat hexadecapeptide, *Biochemistry* **32,** 10,580–10,590 (1993).
17. N. Farrow, R. Muhandiram, A. Singer, S. Pascal, C. Kay, G. Gish, S. Shoelson, T. Pawson, J. Forman-Kay, and L. Kay, Backbone dynamics of a free and phosphopeptide-complexed Src homology 2 domain studied by ^{15}N NMR relaxation, *Biochemistry* **33,** 5984–6003 (1994).
18. L. E. Kay, L. K. Nicholson, F. Delaglio, A. Bax, and D. A. Torchia, Pulse sequences for removal of the effects of cross correlation between dipolar and chemical-shift anisotropy relaxation mechanisms on the measurement of heteronuclear T_1 and T_2 values in proteins, *J. Magn. Reson.* **97,** 359–375 (1992).
19. A. G. Palmer III, N. J. Skelton, W. J. Chasin, P. E. Wright, and M. Rance, Suppression of the effects of cross-correlation between dipolar and anisotropic chemical shift relaxation mechanisms in the measurement of spin-spin relaxation rates, *Mol. Phys.* **75,** 699–711 (1992).
20. S. H. Smallcombe, Solvent suppression with simetrically shifted pulses, *J. Am. Chem. Soc.* **115,** 4769–4785 (1993).
21. T. Tokuhiro and G. Fraenkel, Modulation of spin echoes in multi-half-spin systems. I. Closed formulas of Carr-Purcell spin echoes in several A_aBX_x systems, *J. Chem. Phys.* **49,** 3998–4008 (1968).
22. V. Orekhov, K. Pervushin, and A. Arseniev, Backbone dynamics of (1-71) bacterioopsin studied by two-dimensional ^{1}H-^{15}N NMR spectroscopy, *Eur. J. Biochem.* **219,** 887–896 (1994).
23. J. Loria, M. Rance, and A. Palmer III, Sensitivity improvement of transverse relaxation-optimized spectroscopy, *J. Am. Chem. Soc.* **121,** 2331–2332 (1999).
24. A. J. Shaka, J. Keeler, T. Frenkiel, and R. Freeman, An improved sequence for broadband decoupling: WALTZ-16, *J. Magn. Reson.* **52,** 335–338 (1983).
25. J. L. Markley, W. J. Horsley, and M. P. Klein, Spin-lattice relaxation measurements in slowly relaxing complex spectra, *J. Chem. Phys.* **55,** 3604–3605 (1971).
26. S. Grzesiek and A. Bax, The importance of not saturating H_2O in protein NMR. Application to sensitivity enhancement and NOE measurements, *J. Am. Chem. Soc.* **115,** 12,593–12,594 (1993).
27. V. A. Daragan and K. M. Mayo, Using the model free approach to analyze NMR relaxation data in cases of anisotropic molecular diffusion, *J. Phys. Chem.* **103,** 6829–6843 (1999).
28. L. D. Favro, Asymmetric diffusion tensor for molecular rotations, *Phys. Rev.* **119,** 53–59 (1960).
29. D. E. Woessner, Nuclear spin relaxation in ellipsoids undergoing rotational Brownian motion, *J. Chem. Phys.* **37,** 647–653 (1962).
30. W. T. Huntress, Jr., Effect of anisotropic molecular rotational diffusion on nuclear magnetic relaxation in liquids, *J. Chem. Phys.* **48,** 3524–3534 (1967).
31. R. M. Ballew, J. Sabelko, and M. Gruebele, Direct observation of fast protein folding: The initial collapse of apomyoglobin, *Proc. Natl. Acad. Sci. USA* **93,** 5759–5764 (1996).
32. V. Munoz, P. A. Thompson, J. Hofrichter, and W. A. Eaton, Folding dynamics and mechanism of β-hairpin formation, *Nature* **380,** 196–199 (1997).
33. V. A. Daragan and K. H. Mayo, Analysis of internally restricted correlated rotations in peptides and proteins using ^{13}C and ^{15}N NMR relaxation data, *J. Phys. Chem.* **100,** 8378–8388 (1996).
34. V. Daragan, E. E. Ilyina, C. G. Fields, G. B. Fields, and K. H. Mayo, Backbone and side-chain dynamics of residues in a partially folded β-sheet peptide from platelet factor-4, *Protein Sci.* **6,** 355–363 (1997).
35. M. Ramirez-Alvarado, V. A. Daragan, L. Serrano, and K. H. Mayo, Motional dynamics of residue in a β-hairpin peptide measured by ^{13}C-NMR relaxation, *Protein Sci.* **7,** 720–729 (1998).